Quasi-3D Finite Element Shallow-Water Flow with $k - \epsilon$ Turbulence Model

C. Leupi[(†)], E. Miglio[♭], M. Altinakar[(‡)], A. Quarteroni[(§)], M.O. Deville[(†)].

14th February 2004

[(†)] STI-ISE-LIN, Swiss Federal Institute of Technology, Lausanne 1015, Switzerland
[♭] Politecnico di Milano, Dipartimento di Matematica "F. Brioschi", Piazza Leonardo da Vinci 32, 20133 Milano, Italy.
[(‡)] NCCHE, The University of Mississipi, Carrier Hall Room 102 University, MS 38677 USA.
[(§)] SB-IACS-CMCS, Swiss Federal Institute of Technology, Lausanne 1015, Switzerland.

Abstract

An extension of a three-dimensional (3D) finite element method is proposed for shallow-water equations (SWE). The method is based on the Raviart-Thomas finite element approximation. A numerical solution for shallow-water flows is developed based on the unsteady Reynolds-averaged Navier-Stokes (RANS) equations. In this work the assumption of hydrostatic pressure is applied. The SWE equations are solved in a given multi-layered system (which consists of an a priori subdivision of the vertical direction of the domain into layers of fixed thickness), with a semi-implicit time stepping method. The eddy viscosity is calculated usind the standard $k - \varepsilon$ turbulence model. The boundary conditions at the bed are based on the equilibrium assumption of the production terms with vertical diffusion terms using wall functions. To test the validity of the new algorithm the model is applied to three-dimensional flows for which experimental data and other numerical results are available for comparison.

1 Introduction

The simulation of free surface flows is applied for the description of awide variety of geophysical phenomena like hydrodynamic currents in ocean and coastal engineering in order to simulate tidal currents and transport of pollutants, in meteorology for weather prediction, etc.

Modeling of the hydrodynamics of free surface flows involves the numerical solution of basic conservation equations for mass, momentum and turbulent energy.

The shallow-water equations in depth-averaged form have been successfully applied to many engineering problems and their use has become common practice in environnemental impact studies in estuarial and coastal regions. However in many situations, particulary those involving solute and sediment transport, the vertical variation of velocity is also important and three-dimensional computations, maintaining the hydrostatic pressure assumption, have become a practical proposition over the last decade with increasing computing power.

One of the most intricable problems in hydrodynamics modelling (oceanography, limnography etc...) is an adequate parameterisation of vertical exchange processes. In the present model the latter are represented through the eddy coefficient ν_v whose value is provided by a turbulence model.

The choice of an appropriate turbulence model can affect the accuracy of the results. A large variety of turbulence parameterisations with a substantial range of complexity has been proposed in the literature. Various multiple-level models have been developed in Cartesian space with specified friction at layer interfaces and simple formula for eddy viscosity (see [1], [2]). A similar approach, only using a vertically coupled finite difference scheme, has been studied by Casulli and Cheng using Lagragian advection [3]. Other schemes have been formulated with equations in σ-coordinate form in the vertical (fitted to the bed and the water surface). The ADI scheme has been applied by Uittenbogaard et al.[4] for 3D simulation, and the Casulli and Cheng scheme has been set-up in σ-cordinate by Stansby and Zhou [5], and by Luyten et al. [6].

The level of turbulence modelling required or desirable for a particular application is a rather open question, depending on type of flows and the required features. For example in other engineering areas, notably aeronautical, more advanced anisotropic turbulence modelling has been employed: non-linear $k-\varepsilon$ modelling (see [7]), and full Reynolds stress transport modelling , with a great computational expense. However it should be pointed out that, these flows do not have the complication of a moving free surface with wetting and drying of cells.

The selection of a suitable scheme is often a difficult task since it depends on the type of physical processes specific for simulated area (e.g. tides, thermoclines, river fronts,...), the vertical resolution of the model and the amount of CPU time. In geophysical flows the turbulence manifests itself in various scales. Therefore its modelling is notoriously difficult and even the most advanced second-order and third-order closures have also their deficiencies (see [9], [8]) besides being expensive. Therefore most of the three-dimensional models used in oceanography and physical limnology implement much simpler one- or two-equation turbulence closures. In this work we will use the state-of-the-art $k-\epsilon$ model in the framework of the Reynolds-averaged Navier-Stokes (RANS) equations. Some geophysical applications of this model have been described by Rodi [11].

It should be pointed out that the turbulence equations are generally convection dominated. Therefore the critical problem in the turbulence modelling is the preservation of the positivity of the turbulent kinetic energy, k, and its rate of dissipation, ϵ.

In the present paper, we propose to develop an integrated $k-\epsilon$ two-equation turbulence model around an existing hydrodynamic module based on a recent method for solving quasi three-dimensional (3D) shallow-water equations (SWE) with free surface ([10]). The method uses a mass preserving, unstructured finite element approach in the

horizontal plane. In the vertical direction, the computational domain is divided into a number of layers at predefined heights and the model uses a conventional conforming finite element scheme.

The equations modelling free surface flows are derived from the three-dimensional Navier-Stokes equations and the hydrostatic pressure is assumed with the implication that horizontal pressure gradients are independent of depth, hence only long waves will be taken into account. This means that the vertical accelerations are neglected since the wavelength is much greater than the height of the wave itself.

The so-called *Quasi-3D* models are generated by integrating the continuity equation along the vertical. The horizontal momentum and depth-integrated continuity equations are solved directly, incorporating some form of turbulence model and the vertical velocity is approximated from the (local) continuity equation.

For the turbulence part of the algorithm, the robust formulation of Mohammadi and Pironneau [12] based on the fractional step method is proposed. Combining this method with the characteristics Galerkin method can guarantee the positivity of the solutions and the stability of the scheme.

In the present work, wall functions defined by the bed roughness function are used and wind stress can be considered at the free-surface. The time marching scheme is achieved through a Lagrangian-Galerkin approach (i.e. a characteristics Galerkin method) that has two main features:
- it is an upwind scheme and is therefore well suited for convection-dominated problems;
- it is stable under a mild stability criterion, allowing therefore the use of a large time-step when appropriate.

An outline of this paper is as follows. In section 2, we review the shallow-water equations and the mathematical models for the two-equation $k-\epsilon$ turbulence model, the associated boundary conditions and we derive a weak formulation suitable for the *Quasi-3D* model. In section 3, we introduce the discretization of the physical domain and the finite element approximation. Section 4 treats the temporal discretization based on the Lagragian-Galerkin approach. In section 5 we propose some numerical tests of various complexity in order to verify that the scheme is stable and accurate.

2 Mathematical models for turbulent free surface flows

A detailed description of the hydrodynamic model 3D-ML-SWE (Three Dimensional Multi-Layers Shallow Water Equations) can be found in [10], [13], [14]. A brief description of the hydrostatic version of the model is provided. In this model some modifications have been implemented to account for turbulence effects, such as the introduction of eddy coefficients and wall functions for the bottom boundary conditions.

Figure 1 represents a three-dimensional time varying domain $\widehat{\Omega}$. Let us denote by Ω the projection of $\widehat{\Omega}$ on the xy horizontal plane. The z-axis points in the upward vertical direction. The domain $\widehat{\Omega(t)}$ is bounded by the following surfaces:

- The free-surface Γ_s given by $z = \eta(x, y, t)$,where $\eta(x, y, t)$ represents the elevation of the free-surface with respect to the horizontal reference plane xy.
- The bottom topography Γ_b given by $z = -\mathrm{h}(x, y)$, where $\mathrm{h}(x, y)$ is the distance between the bottom and the horizontal reference plane xy.
- The open-sea boundary denoted by Γ_o.

In this configuration, the total water depth at the point $P(x, y)$ at time t is simply given by

$$H\left(x, y, t\right) = \mathrm{h}\left(x, y\right) + \eta\left(x, y, t\right)$$

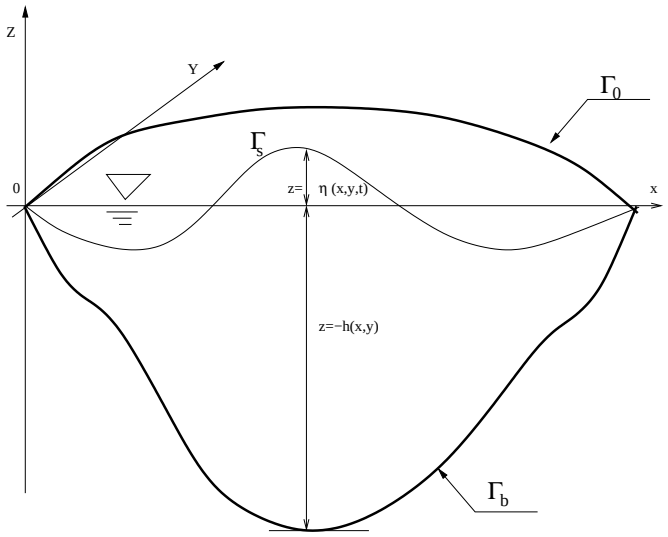

Figure 1: vertical cross section of the domain

where (x, y, z) represents the Cartesian coordinates system.

The fluid motion is described by the Reynolds-averaged Navier-Stokes equations (RANS) namely:

$$\frac{\partial \mathbf{V}}{\partial t} + \left(\mathbf{V} \cdot \nabla\right) \mathbf{V} = -\frac{1}{\rho}\nabla p + \nabla \cdot \left(\nu_v \nabla \mathbf{V}\right) + \mathbf{f}_{xy} \tag{1}$$

$$\nabla \cdot \mathbf{V} = 0 \tag{2}$$

In the previous relations $\mathbf{V} = (u, v, w)^T$ is the $3D$ turbulent velocity vector, $\mathbf{f}_{xy} = (fv, -fu)^T$ is the vector of body forces with f the Coriolis parameter, $\nu_t = (\nu_h, \nu_v)$ is the anisotropic eddy viscosity and $(\nu_h,\ \nu_v)$ are respectively the horizontal and vertical eddy viscosities, see Rodi [18]), $\nabla\cdot$ is the $3D$ divergence operator, ρ is the water density, p is the pressure.

The RANS description of the turbulent motion relies on the Boussinesq approximation([15]). For $t > 0$ and $(x, y, z) \in \widehat{\Omega}(t)$, and using the Boussinesq assumption for the hydrostatic approximation we have that

$$\frac{1}{\rho}\frac{\partial p}{\partial z} = -g \Rightarrow p = p_0 + \rho g\,(\eta - z) \tag{3}$$

where p_0 is the atmospheric pressure. Hence the RANS equations can be written as

$$\nabla \cdot \mathbf{V} = 0 \tag{4}$$

$$\frac{D\boldsymbol{\upsilon}}{Dt} = g\nabla_{xy}\eta + \nabla_{xy}\cdot(\nu_h \nabla_{xy}\boldsymbol{\upsilon}) + \frac{\partial}{\partial z}\left(\nu_v \frac{\partial \boldsymbol{\upsilon}}{\partial z}\right) + \mathbf{f}_{xy} \tag{5}$$

where $\boldsymbol{\upsilon} = (u, v)^T$ is the horizontal velocity vector, g is the gravitational acceleration. ∇_{xy} is the 2D nabla operator, and $\frac{D}{Dt} = \frac{\partial}{\partial t} + (\mathbf{V}\cdot\nabla)$ is the total derivative.

The RANS set will be completed later by integrating the continuity equation over the depth and applying the kinematic free surface condition and the Leibniz rule to give the *depth-integrated* continuity equation.

In eq.(5), the vertical eddy viscosity is defined as

$$\nu_v = c_\mu \frac{k^2}{\epsilon} \tag{6}$$

For the horizontal diffusion, uniform horizontal coefficient can be expressed using the empirical relation.
-The first one from*Elder* [16]

$$\nu_h = \zeta h u_* \tag{7}$$

where ζ it is a constant:e.g $\zeta = 0.1 \;\; to \;\; 0.3$
-The second one for rivers flows from *Shirou Aya*[17]

$$\frac{\nu_h}{h u_*} = 2.0\left(\frac{B}{h}\right)^{\frac{3}{2}} \tag{8}$$

where B is a width of the channel and u_* is a representative shear velocity.

The quantities k and ϵ are described by the following equations ([20], [19]).

$$\frac{Dk}{Dt} - \nabla \cdot \left[c_\mu \frac{k^2}{\epsilon} \nabla k \right] = c_\mu \frac{k^2}{\epsilon} G - \epsilon \tag{9}$$

$$\frac{D\epsilon}{Dt} - \nabla \cdot \left[c_\epsilon \frac{k^2}{\epsilon} \nabla \epsilon \right] = c_1 k G - c_2 \frac{\epsilon^2}{k} \tag{10}$$

The values of the turbulent constants are given: $c_1 = 0.126$, $c_2 = 0.07$, $c_\mu = 0.09$, $c_\epsilon = 1.92$.
The squared shear frequency or production term G is (see [6]):

$$G = \frac{1}{2} \left(\| \nabla \mathbf{V} + \nabla \mathbf{V}^T \| \right)^2 \tag{11}$$

where $\|.\|$ is the $2-$norm of the matrix.

2.1 Boundary and initial conditions

2.1.1 Bottom boundary conditions

At the bottom boundaries the free-slip condition is applied together with a zero normal velocity component to Γ_b. This second condition can be represented by :

$$w_b = u_b \frac{\partial h}{\partial x} + v_b \frac{\partial h}{\partial y} = 0, \qquad \text{on } \Gamma_b \tag{12}$$

Standard wall functions are used as boundary conditions at the bed (see [20]). The logarithmic law of the wall is used to relate the velocity just above the bed to the bed friction velocity $u_* = \sqrt{\tau_0/\rho}$:

$$\frac{u_m}{u_*} = \frac{1}{\kappa} ln \left(E \delta_m^+ \right) \quad \text{, with} \quad \delta_m^+ = \frac{u_* \delta_m}{\nu} \tag{13}$$

where τ_0 is the bed shear stress, $u_m = \sqrt{(u^2 + v^2)}$ at distance δ_m above the bed (i.e in the rough turbulent boundary layer, δ_m is the normal distance to the nearest wall). This wall region is valid for $30 < \delta_m^+ < 100$. In the spatial discretization the first vertical mesh point should thus lie within this region. The shear stress within the wall region may be assumed constant (for a given horizontal location) and for a given vertical position z_1 we have

$$u_* = \frac{u_{m1}}{\{ \frac{1}{\kappa} ln \left(E \delta_{m1}^+ \right) \}} \tag{14}$$

The shear stress components in the horizontal directions τ_{0x} and τ_{0y} are resolved as ([21])

$$\frac{\tau_{0x}}{\rho} = \nu_v \frac{\partial u}{\partial z} = \gamma u_1, \quad \frac{\tau_{0y}}{\rho} = \nu_v \frac{\partial v}{\partial z} = \gamma v_1 \tag{15}$$

where u_1 and v_1 are the velocities at z_1 and

$$\gamma = \frac{u_{m1}}{\{\frac{1}{\kappa} ln\left(E\delta_{m1}^{+}\right)\}^2} \tag{16}$$

The wall roughness coefficient E is adjusted according to the standard roughness,k_s (Wu et al. [22]) by the relation

$$E = \exp\left[\kappa\left(\mathcal{B} - \Delta\mathcal{B}\right)\right] \tag{17}$$

where $\mathcal{B} = 5.2$ is an additive constant, $\Delta\mathcal{B}$ is a roughness function related to k_s, such as (see Cebeci and Bradshaw [23]):

$$\Delta\mathcal{B} = \begin{cases} 0 & \text{for} \quad k_s^+ < 2.25 \\ \left[\mathcal{B} - 8.5 + \frac{1}{\kappa} ln k_s^+\right] sin\left[0.4258\left(ln k_s^+ - 0.811\right)\right] & \text{for} \quad 2.25 < k_s^+ < 90 \\ \mathcal{B} - 8.5 + \frac{1}{\kappa} ln k_s^+ & \text{for} \quad k_s^+ > 90 \end{cases} \tag{18}$$

where $k_s^+ = \frac{u_* k_s}{\nu}$ is the roughness Reynolds number, $\kappa = 0.41$ is von Karman's constant .

Remark 1 *It is worthwhile to notice that the coefficient E in the above relation accounts for all flow regimes, either hydraulically smooth, rough, or transitional.*

The production of the turbulent kinetic energy is merely due to the (turbulent) shear stress.

At the bottom the equilibrium assumption is adopted (i.e local balance between production of turbulent kinetic energy and the rate of dissipation [20],[15]).

$$k_m = \frac{u_*^2}{(c_\mu)^{\frac{1}{2}}} \tag{19}$$

$$\epsilon_m = \frac{(c_\mu)^{\frac{3}{4}} (k_m)^{\frac{3}{2}}}{\kappa \delta_m} \tag{20}$$

2.1.2 Free surface boundary conditions

The wind stress on Γ_s is given by

$$\nu_v \frac{\partial \boldsymbol{v}}{\partial z} = \rho_a C_w \|W\| W \tag{21}$$

with C_w being a constant whose value depends on the wind speed and $\|W\|$ denoting the module of the wind velocity at $10[m]$ above the free-surface. The symbol ρ_a is the air density.

At the free-surface, Γ_s, the kinematic condition states that the fluid particles at the free surface move with the free surface :

$$w_s = \frac{\partial \eta}{\partial t} + u_s \frac{\partial \eta}{\partial x} + v_s \frac{\partial \eta}{\partial y} \qquad \text{on } \Gamma_s \tag{22}$$

Then integrating the continuity equation in the z direction and using the kinematic boundary condition we obtain the following equation describing the evolution of the free-surface

$$\frac{\partial \eta}{\partial t} + \nabla_{xy} \cdot \left(\int_{-h(x,y)}^{\eta(x,y)} \boldsymbol{v} dz \right) = 0 \tag{23}$$

The boundary conditions for turbulent quantities (see Stansby and Zhou [5]) are :

$$\frac{\partial k}{\partial z} = 0 \tag{24}$$

$$\epsilon = \frac{(k c_\mu)^{1.5}}{0.07 \kappa h} \tag{25}$$

where $c_\mu = 0.09$ is a model constant.

2.1.3 Open sea, river outlet and vertical wall boundary conditions

At the open sea or outlet boundary denoted by Γ_o, the water depth is a known function of time and Neumann natural boundary conditions are applied for the velocity ($\frac{\partial \boldsymbol{v}}{\partial n} = 0$), and other variables (i.e. a zero normal gradient through these surfaces), where $\frac{\partial}{\partial n}$ is the normal derivative to the surface. At the vertical wall, the slip boundary conditions are used by setting all normal components to the vertical wall equal to zero ($\boldsymbol{v}_n = 0$), and Neumann boundary conditions are applied for turbulent quantities:

$$\frac{\partial k}{\partial n} = 0 \quad , \quad \frac{\partial \epsilon}{\partial n} = 0 \tag{26}$$

2.1.4 Inlet boundary (or upstream)

The given known functions describes the flow

$$Q = f\left(x, y, t\right) \tag{27}$$
$$V = f\left(Q, H_{inl}\right) \tag{28}$$
$$k = 0.03u^2 \tag{29}$$
$$\epsilon = c_\mu \frac{k^{1.5}}{0.09h} \tag{30}$$

where Q denotes a prescribed discharge, u is the x component of the velocity $\mathbf{V}$, H_{inl} is the water depth at inlet.

2.1.5 Initial conditions

The initial conditions for velocities and free-surface can be written:

$$V = V_0 \quad ; \quad \eta = \eta_0 \tag{31}$$

The initial values of turbulent quantities : (see Versteeg and Malalasekera [24]):

$$k = 1.5(0.06U)^2 \tag{32}$$
$$\epsilon = \frac{{c_\mu}^{3/4} k^{3/2}}{0.09h} \tag{33}$$

where U is the known value of Uniform distribution velocity.

3 Space discretization

In the sequel the finite element method is used to discretize in space the advection-diffusion equations of the turbulent quantities. Let us introduce some details for the computational purpose. Figure 2 represents the physical domain. A three-dimensional region is embedded in a parallelepiped composed of $\mathcal{N}$ layers. By $\mathcal{I}_k$ we identify the layer k whose thickness δz_k is fixed. A layer is said to be active if it is wet. The number of active layers is not constant over the whole domain and can also change in time, accounting for the variation of the free surface. In particular the thickness of the lower-most active layer (denoted by the index k_0) depends on the bottom shape, while the thickness of the uppermost active layer (whose index is $\mathcal{K}$) varies in space and time according to the free surface location.

The horizontal projection of the domain Ω is discretised using an unstructured triangular mesh $\mathcal{T}_h$. The same mesh is placed in the middle of each layer. The vertical distance between the grids of the layers k and $k+1$ will be denoted by $\delta z_{k+1/2} = [\delta z_k + \delta z_{k+1}]/2$. In each layer, each triangular mesh element defines a three-dimensional prismatic element. The horizontal components of the velocity vector are defined at the middle of edges of the triangular mesh elements, while the vertical components are associated with the lower horizontal face of the element in the case of hydrostatic pressure assumption.

Let us introduce some functional spaces that will be used in this work. Let $\Omega \subset \mathbb{R}^d$, then:

$$L^2(\Omega) = \left\{ \psi : \int_\Omega \psi^2 \mathrm{d}\Omega < \infty \right\} \tag{34}$$

$$H^1(\Omega) = \left\{ \psi \in L^2(\Omega) : \partial_{x_i}\psi \in L^2(\Omega), \mathrm{i} = 1, \ldots, \mathrm{d} \right\} \tag{35}$$

The following space of vectors have been introduced to derive the weak form of the quasi-3D hydrodynamic model:

$$H_{o,c}(div;\Omega) = \{ \boldsymbol{\tau} : \boldsymbol{\tau} \in \left(L^2(\Omega)\right)^2, div\,\boldsymbol{\tau} \in L^2(\Omega), \boldsymbol{\tau} \cdot \mathbf{n} = 0 \text{ on } \Gamma_c \} \tag{36}$$

where Γ_c denote the vertical solid wall.

For every integer $r \geq 0$ we denote by $\mathbb{P}_r(T)$ the space of polynomials of degree $\leq r$ on each triangle $T \in \mathcal{T}_h$ (see figure 2) and consider the Raviart-Thomas vector finite element space of lowest order (see [13], [25]):

$$\mathbb{RT}_0(T) = (\mathbb{P}_0(T))^2 \oplus \mathbf{x}\mathbb{P}_0(T) = \left\{ \boldsymbol{\upsilon} = \begin{pmatrix} b \\ c \end{pmatrix} + a \begin{pmatrix} x \\ y \end{pmatrix},\ a, b, c \in \mathbb{R} \right\}. \tag{37}$$

Let us introduce the following finite element spaces :

$$\mathbb{Q}_h = \{\mathbf{q} \in \mathrm{H}_{0,c}(\mathrm{div}; \Omega) : \mathbf{q}|_T \in \mathbb{RT}_0(T),\ \forall T \in \mathcal{T}_h\},$$

$$U_h = \{\psi \in L^2(\Omega) : \psi|_T \in \mathbb{P}_0(T)\},$$

$$W_{\delta z} = \{\varphi \in \mathrm{H}^1([-\mathfrak{h}, \eta]) : \varphi|_{\mathcal{I}_k} \in \mathbb{P}_1(\mathcal{I}_k)\}.$$

$$X_p = \{\chi \in L^2(\Omega) : \chi|_p \in \mathbb{P}_0(p), \forall p\}$$

We will approximate k and ϵ by piecewise constant functions on each prism p, respectively. Let us consider a generic characteristic function χ for each prism such that $\chi \in X_p$. To approximate the system of Eqs. (4), (23, (5) and using the divergence formula and the boundary conditions from eq.(13), (21) the problem statement is now:
Find $\boldsymbol{\upsilon} \in Q_h \times W_{\delta z}$, $w \in X_p$,$\eta \in X_p$, $k \in X_p$, $\epsilon \in X_p$, such that :

$$\int_{\partial p} w n_z ds = \int_{\partial p} \boldsymbol{\upsilon} \cdot \mathbf{n}_{xy} \mathrm{d}S, \qquad \forall p \tag{38}$$

$$\int_\Omega \frac{\partial \eta}{\partial t} \psi \mathrm{d}\Omega + \int_\Omega \left(\nabla_{xy} \cdot \int_{-\mathfrak{h}}^{\eta} \boldsymbol{\upsilon} \mathrm{d}z \right) \psi \mathrm{d}\Omega = 0 \qquad \forall \psi \in U_h \tag{39}$$

$$\begin{aligned} \int_\Omega \int_{-\mathfrak{h}}^{\eta} \varphi \frac{D\boldsymbol{\upsilon}}{Dt} \cdot \boldsymbol{\tau} \mathrm{d}z \mathrm{d}\Omega &= g \int_\Omega \int_{-\mathfrak{h}}^{\eta} \varphi \eta \nabla_{xy} \cdot \boldsymbol{\tau} \mathrm{d}z \mathrm{d}\Omega + \nu_h \int_{\partial\Omega} \int_{-\mathfrak{h}}^{\eta} \varphi \nabla_{xy} \boldsymbol{\upsilon} \cdot \boldsymbol{\tau} \mathrm{d}z \mathrm{d}S \\ &- \nu_v \int_\Omega \int_{-\mathfrak{h}}^{\eta} \boldsymbol{\tau} \cdot \frac{\partial \boldsymbol{\upsilon}}{\partial z} \frac{\partial \varphi}{\partial z} \mathrm{d}z \mathrm{d}\Omega + \int_\Omega \int_{-\mathfrak{h}}^{\eta} \varphi \mathbf{f}_{\mathrm{xy}} \cdot \boldsymbol{\tau} \mathrm{d}z \mathrm{d}\Omega \\ &+ \int_\Omega \left[(\rho_a C_w \|W\| W \cdot \boldsymbol{\tau} \varphi) \,|_\eta - \gamma u_m \cdot \boldsymbol{\tau} \varphi|_{\mathfrak{h}} \right] \mathrm{d}\Omega \\ &- g \int_{\Gamma_0 \cap \Gamma_b} \int_{-\mathfrak{h}}^{\eta} \varphi \eta \boldsymbol{\tau} \cdot \mathbf{n} \mathrm{d}z \mathrm{d}\gamma, \qquad \forall \boldsymbol{\tau} \in \mathbb{Q}_h, \forall \varphi \in W_{\delta z} \end{aligned} \tag{40}$$

where $\mathbf{n}_{xy}, n_z$ are respectively the horizontal and vertical components of the normal vector $\mathbf{n}$.
Denoting by Ned and Nel the number of oriented edges e_l and triangles T_j in the mesh, the approximate solution for the horizontal velocity is represented as follows:

$$\boldsymbol{\upsilon} = \sum_{k=k_0}^{\mathcal{K}} \sum_{l=1}^{Ned} (J_l)_k \boldsymbol{\tau}_l (\mathbf{x}) \varphi_k (z) \tag{41}$$

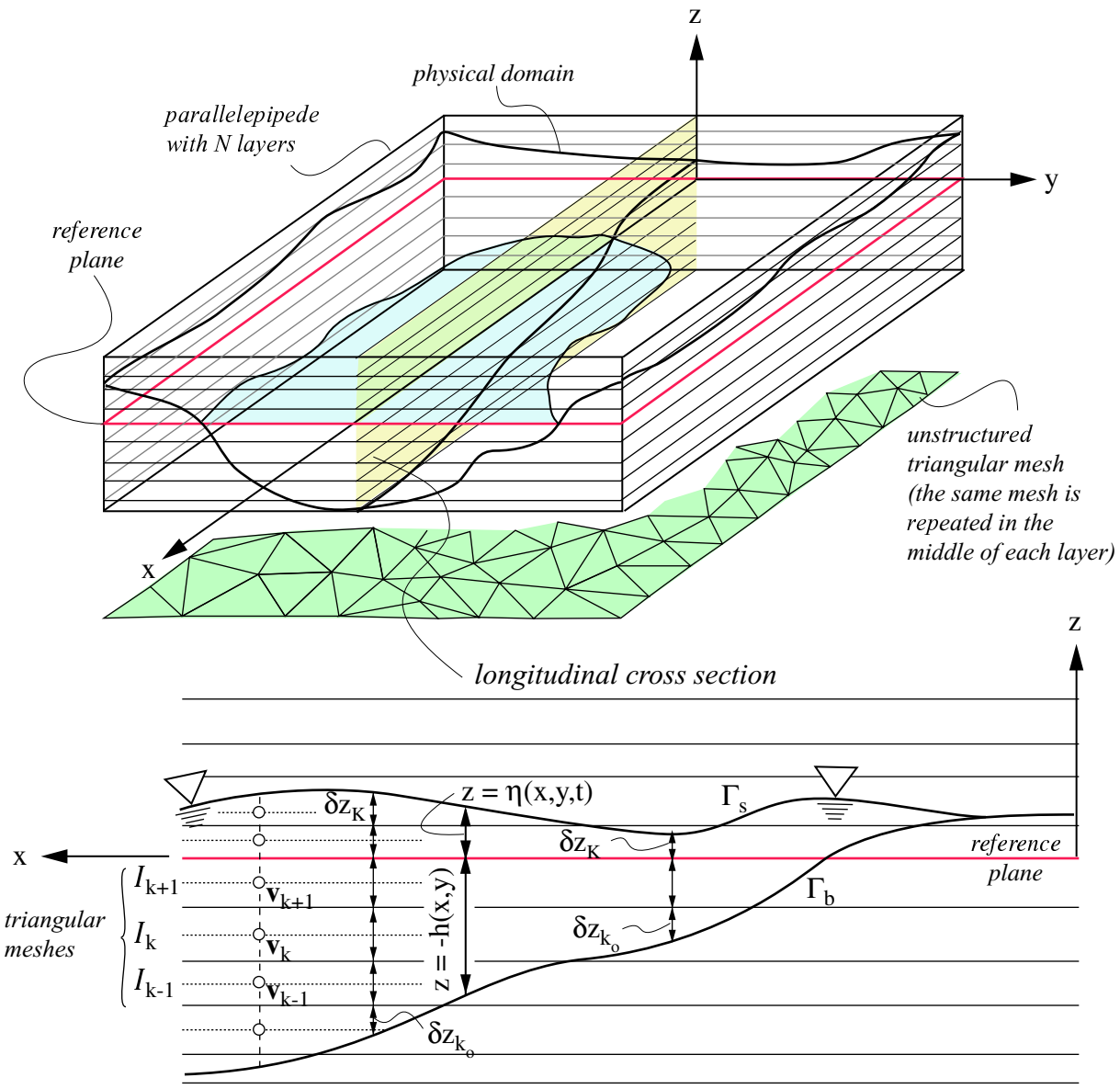

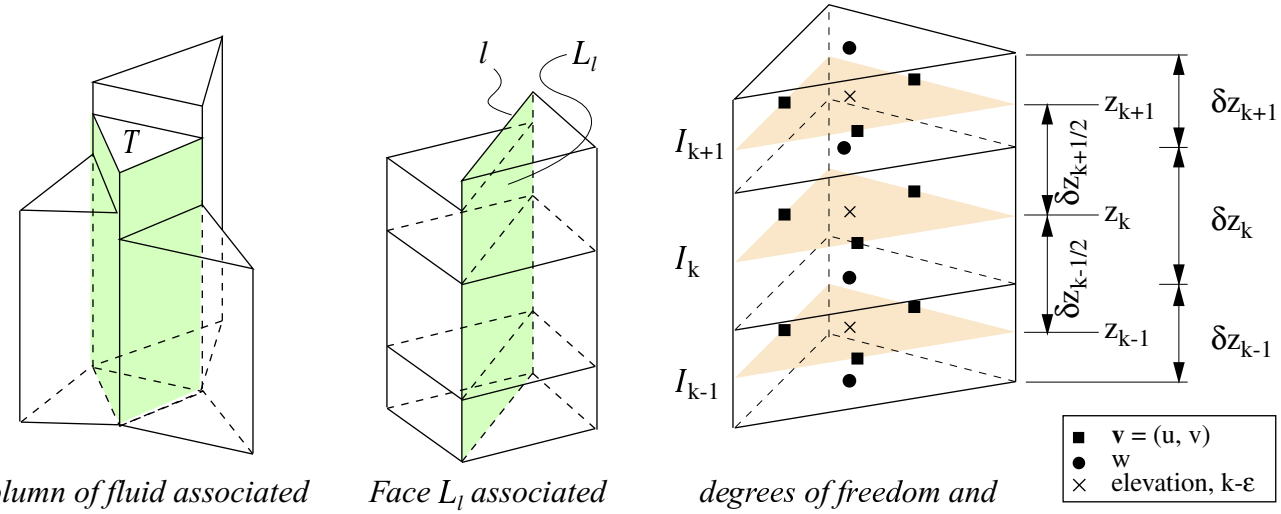

column of fluid associated to the triangle T

Face L_l associated to the edge l

degrees of freedom and definition of layer thicknesses

Figure 2: physical domain

We approximate the elevation by piecewise constant functions on each triangle, so we can write:

$$\eta_h(\mathbf{x}) = \sum_{j=1}^{Nel} \eta_j \psi_j(\mathbf{x}), \tag{42}$$

where $(J_l)_k = \int_{e_l} \boldsymbol{\upsilon}_k \cdot \mathbf{n}\, d\sigma, l = 1, \ldots, Ned$, $\boldsymbol{\tau}_l \in \mathbb{Q}_h$ and $\varphi_k \in W_{\delta z}$, $\mathbf{x} = (x, y)$. $\eta_j = \eta_h|_{T_j}, j = 1, .., Nel$ and $\psi_j \in U_h$.
The approximate solutions for k and ϵ , are given by the relations :

$$k_h(\mathbf{x}, z) = \sum_{j=1}^{Np} k_j \chi_j(\mathbf{x}, z) \tag{43}$$

$$\epsilon_h(\mathbf{x}, z) = \sum_{j=1}^{Np} \epsilon_j \chi_j(\mathbf{x}, z) \tag{44}$$

where Np is the total number of active prisms and χ_j denotes the characteristic function of the j^{th} prism.

Integrating Eq.(9) and (10) over the prism and using Gauss theorem one can write:

$$|P| \frac{Dk_h}{Dt} + |T| \left[c_\mu \frac{k_h^2}{\epsilon_h} \nabla k_h \right] \cdot \mathbf{n} = |p| \left(c_\mu \frac{k_h^2}{\epsilon_h} G - \epsilon_h \right), \quad \forall p \tag{45}$$

$$|P| \frac{D\epsilon_h}{Dt} - |T| \left[c_\epsilon \frac{k_h^2}{\epsilon_h} \nabla \epsilon_h \right] \cdot \mathbf{n} = |p| \left(c_1 k_h G - c_2 \frac{\epsilon_h^2}{k_h} \right), \quad \forall p \tag{46}$$

where $|P|$ and $|T|$ denotes respectively the volume and the surface of the based triangle of the prism p.

4 Temporal discretization

Let us introduce the fully discrete space-time approximations from the Eq.(38)-(40), (45)-(46).

The overall time discretization method is based on the following assumptions:
- the vertical diffusive terms in the advection-diffusion equation are discretized implicitly;
- the source terms are discretised explicitly, while the sink terms are linearized.
- Lagrange-Galerkin (or characteristics Galerkin) approach is used (see [13], [12]) to discretize the material derivative in Eqs.(40), (45) and (46) such that $\Psi\left(\mathbf{X}^n\right) = \Psi\left(\tau, \mathbf{X}\left(\tau; t, \mathbf{x}\right)\right)$ $\forall \tau \in [t^n, t^{n+1}]$.

Let us consider the total derivative:

$$\frac{Dk}{Dt}(t, \mathbf{x}) = \frac{\partial k}{\partial t} + (\mathbf{V} \cdot \nabla)\, k = \frac{\partial}{\partial \tau} k(\tau, \mathbf{X}(\tau; t, \mathbf{x})) \tag{47}$$

where $\mathbf{X}(\boldsymbol{\tau}; t, \mathbf{x})$ is the solution of the following problem:

$$\left\{ \begin{array}{l} \dfrac{d\mathbf{X}\left(\tau; t, \mathbf{x}\right)}{d\tau} = \mathbf{V}\left(\tau, \mathbf{X}\left(\tau; t, \mathbf{x}\right)\right) \text{ for } \tau \in (0, t)\,, \\ \mathbf{X}\left(t; t, \mathbf{x}\right) = \mathbf{x}. \end{array} \right\}. \tag{48}$$

From a geometric point of view $\mathbf{X}\left(\cdot\right) = \mathbf{X}\left(\cdot; t, \mathbf{x}\right)$ is the parametric representation of the trajectories: $\mathbf{X}(\tau; t, \mathbf{x})$ is the position at time τ of a particle which has been driven by the field $\mathbf{V}(u, v, w)$ and that occupied the position $\mathbf{x}$ at time t.
Problem (48) is a system of ordinary differential equations. For its discretization it is possible to use a backward Euler scheme, or a more accurate fourth-order Runge-Kutta scheme. Since (48) is non-linear, to compute $\mathbf{X}\left(t_n; t_{n+1}, \mathbf{x}\right)$ we will use the velocity at time t_n.

The total derivative can be discretized as follows:

$$\frac{Dk}{Dt}(t_{n+1}, \mathbf{x}) \simeq \frac{k\left(t_{n+1}, \mathbf{x}\right) - k\left(t_n, \mathbf{X}\left(t_n; t_{n+1}, \mathbf{x}\right)\right)}{\Delta t}. \tag{49}$$

From the semi-discrete form of the above partial differential equations and using first-order Euler implicit scheme we can write:

Find $\boldsymbol{\upsilon} \in Q_h \times W_{\delta z}$, $w \in X_p$,$\eta \in X_p$, $k \in X_p$, $\epsilon \in X_p$, such that :

$$\int_{\partial p} w^{n+1} n_z ds = \int_{\partial p} \boldsymbol{\upsilon}^{n+1} \cdot \mathbf{n}_{xy} \mathrm{d}S, \qquad \forall p \tag{50}$$

$$\int_{\Omega} \frac{\eta^{n+1} - \eta^n}{\Delta t} \psi \mathrm{d}\Omega + \int_{\Omega} \left(\nabla_{xy} \cdot \int_{-\mathfrak{h}}^{\eta^n} \boldsymbol{\upsilon}^{n+1} \mathrm{d}z \right) \psi \mathrm{d}\Omega = 0 \qquad \forall \psi \in U_h \tag{51}$$

$$\begin{aligned}
\int_\Omega \int_{-\mathfrak{h}}^{\eta^n} \varphi \frac{\boldsymbol{\upsilon}^{n+1} - \boldsymbol{\upsilon}\left(X^n\right)}{\Delta t} \cdot \boldsymbol{\tau} \mathrm{d}z\mathrm{d}\Omega &= g \int_\Omega \int_{-\mathfrak{h}}^{\eta^n} \varphi \eta^{n+1} \nabla_{xy} \cdot \boldsymbol{\tau} \mathrm{d}z\mathrm{d}\Omega \\
&+ \nu_h^n \int_{\partial\Omega} \int_{-\mathfrak{h}}^{\eta^n} \varphi \nabla_{xy} \boldsymbol{\upsilon}^{n+1} \cdot \boldsymbol{\tau} \mathrm{d}z\mathrm{d}S \\
&- \nu_v^n \int_\Omega \int_{-\mathfrak{h}}^{\eta^n} \boldsymbol{\tau} \cdot \frac{\partial \boldsymbol{\upsilon}^{n+1}}{\partial z} \frac{\partial \varphi}{\partial z} \mathrm{d}z\mathrm{d}\Omega + \int_\Omega \int_{-\mathfrak{h}}^{\eta^n} \varphi \mathbf{f}_{\mathrm{xy}}^{\mathrm{n}} \cdot \boldsymbol{\tau} \mathrm{d}z\mathrm{d}\Omega \\
&+ \int_\Omega \left[\left(\rho_a C_w \|W\| W \cdot \boldsymbol{\tau} \varphi\right)|_{\eta^n} - u_m^{n+1} \cdot \boldsymbol{\tau} \varphi|_{\mathfrak{h}} \right] \mathrm{d}\Omega \\
&- g \int_{\Gamma_0 \cap \Gamma_b} \int_{-\mathfrak{h}}^{\eta^n} \varphi \eta^{n+1} \boldsymbol{\tau} \cdot \mathbf{n} \mathrm{d}z\mathrm{d}\gamma, \qquad \forall \boldsymbol{\tau} \in \mathbb{Q}_h, \forall \varphi \in W_{\delta z}
\end{aligned} \tag{52}$$

For the boundary condition at the bottom the non-linear terms in in Eq.(52 has been linearized considering the modulus of the velocity at time n.
The turbulent viscosity ν_v is computed according to the following expression

$$\nu_v^{n+1} \mathrm{d}p = c_\mu \frac{\left(k^{n+1}\right)^2}{\epsilon^{n+1}} \tag{53}$$

The discrete form of Eq.(45) and (46) reads :

$$\begin{aligned}
|P| \frac{\left(k_h^{n+1} - k_h\left(\mathbf{X}^n\right)\right)}{\Delta t} &= |T| \left[c_\mu \frac{{k_h^n}^2}{\epsilon_h^n} \nabla {k_h}^{n+1} \right] \cdot \mathbf{n} \\
&+ |P| \left(c_\mu \frac{{k_h^n}^2}{\epsilon_h} G^n - \frac{\epsilon_h^n}{k_h^n} k_h^{n+1} \right)
\end{aligned} \tag{54}$$

$$|P| \frac{\left(\epsilon_h^{n+1} - \epsilon_h\left(\mathbf{X}^n\right)\right)}{\Delta t} = |T| \left[c_\epsilon \frac{{k_h^2}^n}{\epsilon_h^n} \nabla \epsilon_h^{n+1} \right] \cdot \mathbf{n} + |P| \left(c_1 k_h^n G^n - c_2 \frac{\epsilon_h^n}{k_h^n} \epsilon_h^{n+1} \right) \tag{55}$$

Due to the contribution of the production and diffusive terms that can give rise to instability in the numerical scheme (see [12], [18], it become very difficult to obtain a stable scheme for the set of convection-diffusion equations which preserves positivity of k and ϵ . Using the fractional step algorithm proposed by Mohammadi and Pironneau([12]) for the turbulence model and the method of characteristics for the convective terms allow to ensure the positivity of k and ϵ and the stability of the scheme.

5 A stable semi-implicit fractional-step scheme

The main idea of this algoritm is to split the system of equations into the convection step and the diffusion step. We firstly solve the convective step by using the characterics Galerkin for the convection terms then we solve the diffusion step using the θ projection method (e.g. Crank Nicolson). Therefore the maximum principle for partial differential equations in the discrete case insures positive k, ϵ.

Following this idea and using Gauss formula the k and ϵ equations reads:
Projection step

$$|P|\left(\frac{k_h^{n+\frac{1}{2}}-k_h\left(X^n\right)}{\Delta t}\right)+|T|\left(k_h^{n+\frac{1}{2}}\frac{\epsilon_h^n}{k_h^n}\right)=|P|\,c_\mu\frac{k_h^{n2}}{\epsilon_h^n}G^n \tag{56}$$

$$|P|\left(\frac{\epsilon_h^{n+\frac{1}{2}}-\epsilon_h\left(X^n\right)}{\Delta t}\right)+|T|\left(c_2\epsilon_h^{n+\frac{1}{2}}\frac{\epsilon_h^n}{k_h^n}\right)=|P|\left(c_1k_h^nG^n\right) \tag{57}$$

Correction step

$$|P|\left(\frac{k_h^{n+1}-k_h^{n+\frac{1}{2}}}{\Delta t}\right)+|T|\,\theta\left[c_\mu\left(\frac{k_h^2}{\epsilon_h}\right)^n\nabla k_h^{n+1}+\left(1-\theta\right)c_\mu\left(\frac{k_h^2}{\epsilon_h}\right)^n\nabla k_h^n\right]=0 \tag{58}$$

$$|P|\left(\frac{\epsilon_h^{n+1}-\epsilon_h^{n+\frac{1}{2}}}{\Delta t}\right)+|T|\,\theta\left[c_\epsilon\left(\frac{k_h^2}{\epsilon_h}\right)^n\nabla \epsilon_h^{n+1}+\left(1-\theta\right)c_\epsilon\left(\frac{k_h^2}{\epsilon_h}\right)^n\nabla \epsilon_h^n\right]=0 \tag{59}$$

It is easy to find that the stiffness system matrices for the convective step of Eq.(56) and Eq.(57) are diagonal matrices.

For the diffusion step (see Eq. (58) and (59)), we denote by M the stiffness matrices of each linear system. For each basis triangle $\mathcal{T}_t$ (basis of a generic prism) with $t = 1, ..., Nelm$ on the vertical direction ($Nelm$ denotes the number of basis triangle on the vertical direction). Using the θ projection method for time integration with $\theta \in [0, 1]$, one obtains the following system :

$$\mathbf{M}^g\mathbf{k}^{n+1}=\mathbf{M}^d\mathbf{k}^n+\mathbf{E} \tag{60}$$

where $\mathbf{M}^d$ is a counterpart of the left matrix $\mathbf{M}^g$ of the system due to the projection method. The matrix reads

$$\mathbf{M}^g=\begin{bmatrix}
\Lambda_{\mathcal{K}}+\alpha_{\mathcal{K}} & -\alpha_{\mathcal{K}} & \cdots & 0 & 0\\
-\alpha_{\mathcal{K}-1} & \left(\Lambda_{\mathcal{K}-1}+\alpha_{\mathcal{K}}+\alpha_{\mathcal{K}-1}\right) & -\alpha_{\mathcal{K}-1} & \cdots & 0\\
\vdots & \ddots & \ddots & \ddots & \vdots\\
0 & \cdots & -\alpha_{k_0+2} & \left(\Lambda_{k_0+2}+\alpha_{k_0+2}+\alpha_{k_0+1}\right) & -\alpha_{k_0+1}\\
0 & \cdots & \cdots & -\alpha_{k_0+1} & \Lambda_{k_0+1}+\alpha_{k_0+1}
\end{bmatrix}$$

$$\mathbf{k}^{n+1} = \begin{bmatrix} k_{\mathcal{K}}^{n+1} \\ k_{\mathcal{K}-1}^{n+1} \\ \vdots \\ k_{k_0+1}^{n+1} \\ k_{k_0}^{n+1} \end{bmatrix} \quad ; \quad \mathbf{E} = \Delta t \begin{bmatrix} \beta_{\mathcal{K}} + G_{\mathcal{K}}^{k} \\ G_{\mathcal{K}-1}^{k} \\ \vdots \\ G_{k_0+1}^{k} \\ \beta_{k_0} + G_{k_0}^{k} \end{bmatrix}$$

where $\beta_{\mathcal{K}}$ and β_{k_0} represents the boundary conditions respectively at the free surface and the bottom, $\mid V_p \mid$ is the volume of the prism p and the following auxiliary variables have been introduced

$$\Lambda = k\left(\mathbf{X}^n\right) + c_\mu \frac{k_h^2}{\epsilon_h^n} \frac{\mid e_l \mid}{d_l},$$

$$\alpha_k = \left(c_\mu \frac{k_h^{n2}}{\epsilon_h^n} \delta z_{k-\frac{1}{2}} \right) \Delta t. \tag{61}$$

The respective stiffness matrices for k and ϵ are symmetric and positive definite. Therefore one can efficiently use the preconditioned conjugate gradient solver.

Method of solution

- The horizontal velocity field is described using lowest order Raviart-Thomas finite elements together with a special technique of numerical integration. This technique guarantees a high degree of mass conservation. The time marching scheme for the hydrodynamic part is achieved through a Lagrange-Galerkin approach. The principal advantage of this method is that, owing to the Lagrangian (i.e., non-local) nature of the advection step, the CFL restriction is eliminated.

- The use of the conservative scheme is particularly desirable for scalar transport. Upwinding is implemented via the characteristic Galerkin method. This method is suitable for the relatively large time step, allow the positivity of $k - \epsilon$ and stability of the algorithm.

- The solution procedure for a given time step is as follows:

  1. set the initial values for all variables (u,v,w,η,k,ϵ), or use the values from previous time step.
  2. compute ν_v from Eq.(53) and ν_h from (7 or 8)
  3. solve the free-surface to obtain η, Eq.(51)
  4. solve momentum Eq.(52) to obtain (u,v) and (50) to obtain w

5. solve convective step for k, Eq.(56)
6. solve convective step for ϵ, Eq.(57)
7. solve diffusion step to obtain k, Eq.(58)
8. solve diffusion step to obtain ϵ, Eq.(59)

6 Numerical results

Detailed experimental data for testing the solver are limited. However in order to check the validity of the model developed, the computation was carried out for simulating open channel flows. Therefore two cases of steady and unsteady flow in open channels will be used to test our numerical scheme. The test results will be compared to experimental data for the steady open channel flow which is the ideal case (see [26]), and for the unsteady open channel flow (see [27]), for the water surface profile along the channel and the vertical distributions of the velocity, eddy viscosity, and shear stress.

6.1 Steady flow

The channel layout and dimension is shown in Fig. 5. The discharge is set to $Q = 0.25[m^3/s]$, the bed slope $S_0 = 0.000624$. The rough bed is characterized by an equivalent roughness height, $k_s = 0.0042[m]$. The flow depth at the outflow (donwstream end of the flume) is $0.183[m]$. The experimental data are available for the flow case (see Istiarto [26]). The grid is composed of 5044 elements and 2733 nodes. The time step is set to 0.1s, and the computation is performed till a steady state is reached. The model produces the logarithmic velocity distribution as expected for uniform flows. The computed eddy viscosity profile compares favorably with the experimental one. The eddy viscosity goes to zero near the free-surface, increases with the depth and presents a maximum around the mid-depth, and then, decreases towards zero near the bed. The shear stress profile is linearly distributed with the depth, from zero at free surface to maximum near the bed.

6.1.1 Uniform inlet velocity distribution

The following Fig. 6 shows the water surface. Figure (7a) shows the steady state distributions of the velocities at selected sections , and figure (7b) compares the computed and measured distributions of the velocity, the eddy viscosity, and the shear stress at half reach of the channel, $x = 19.040[m]$. The water surface shows a decreasing flow depth in the first 8-meter reach. Further downstream the flow depth gradually increases towards the specified depth of $h = 0.183[m]$ at the outlet boundary. Within the downstream half channel-reach, $x \geq 20[m]$, a nearly uniform flow-depth is observed, showing less than 1 [mm] difference between the two ends of this channel reach. As shown in figure (6), the computed solutions agree quite well with the experimental data.

6.1.2 Logarithmic inlet velocity distribution

The logarithmic velocity distribution prevails consistenly along the computational domain. The results in figures (8)-(11) shows the applicability of the model to achieve a near perfect agreement between computed and measured steady state free-surface profile and velocity distributions.

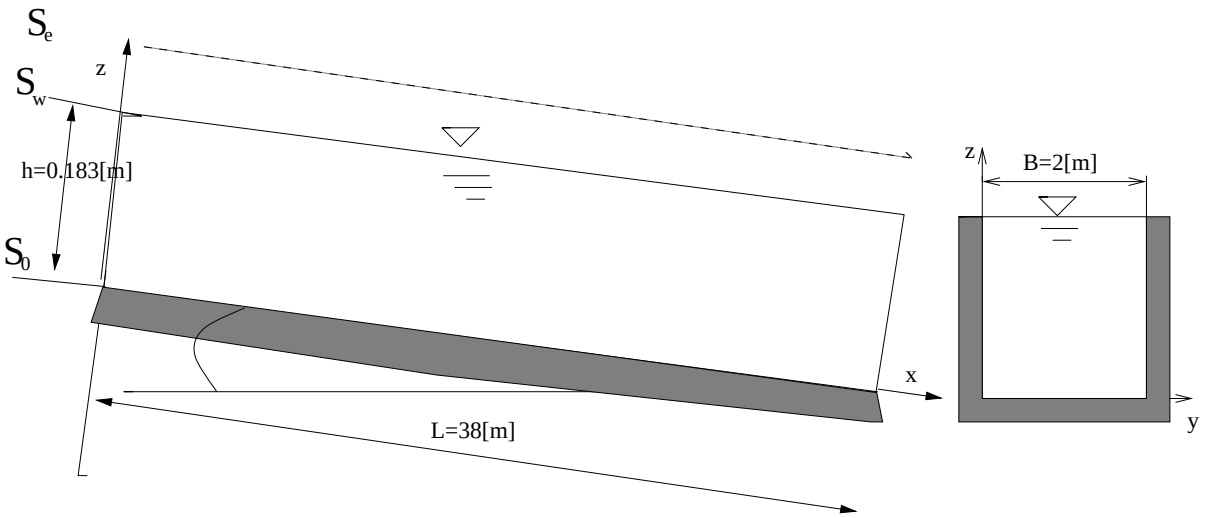

figur 5 Steady uniform flow over open− channel

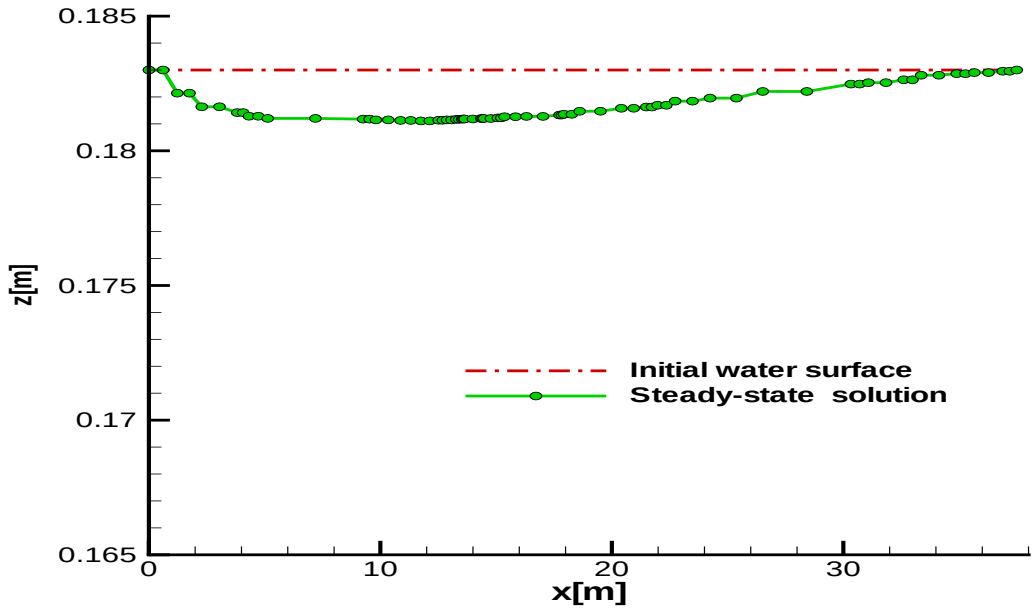

figure 6 Comparison between steady−state solution and initial water surface

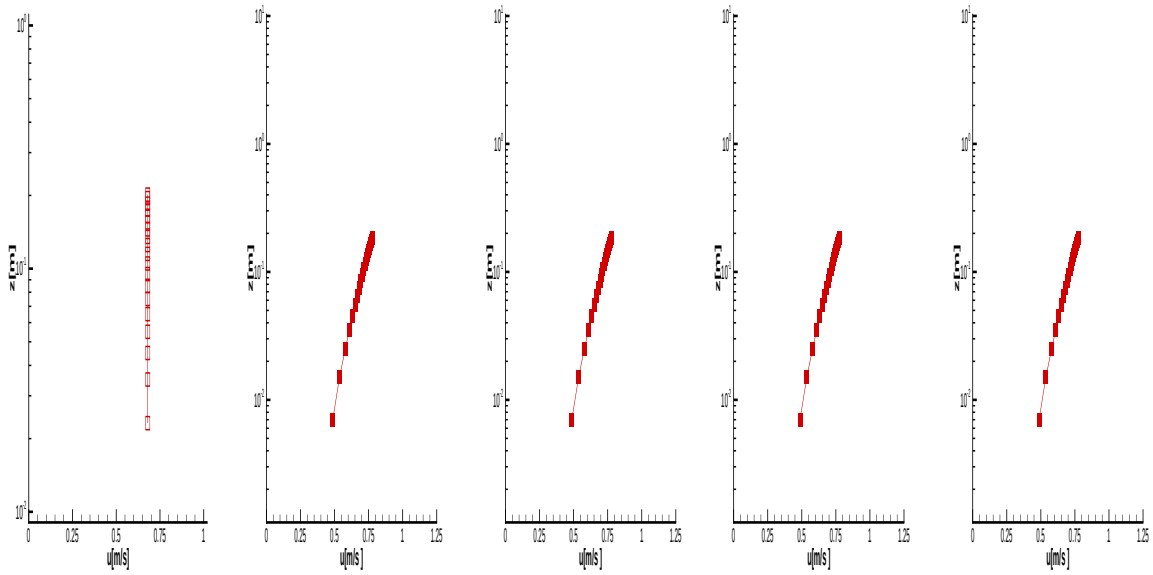

x=0.01[m] x=9.23[m] x=19.04[m] x=28[m] x=37.8[m]

figure 7a. Steady state velocities distributions at selected sections

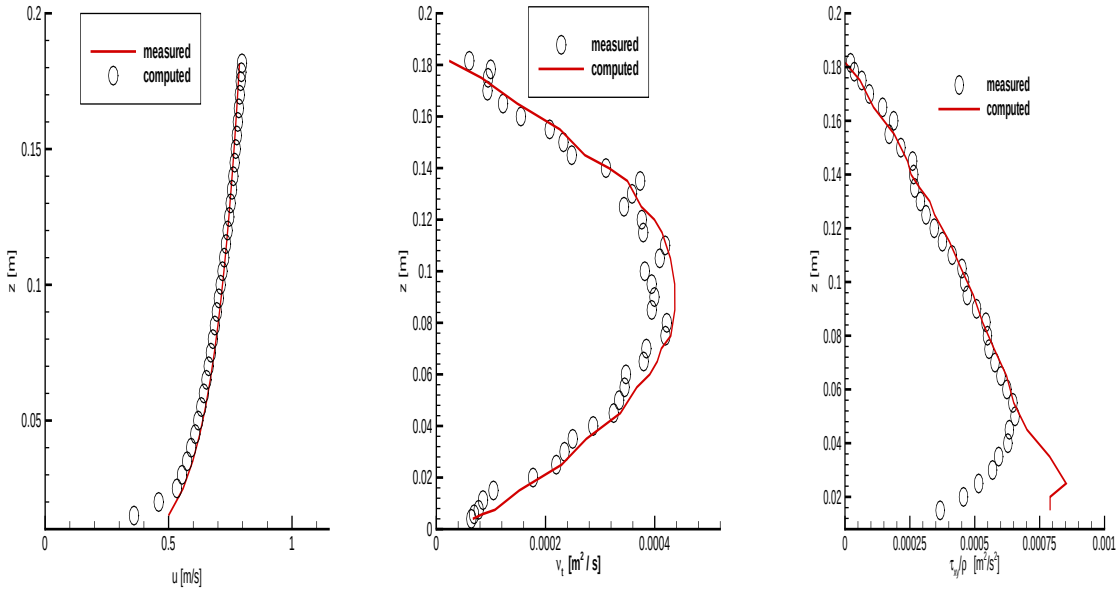

figure 7b. Comparison betwween computed and measured distributions of velocity, eddy viscosity and shear stress

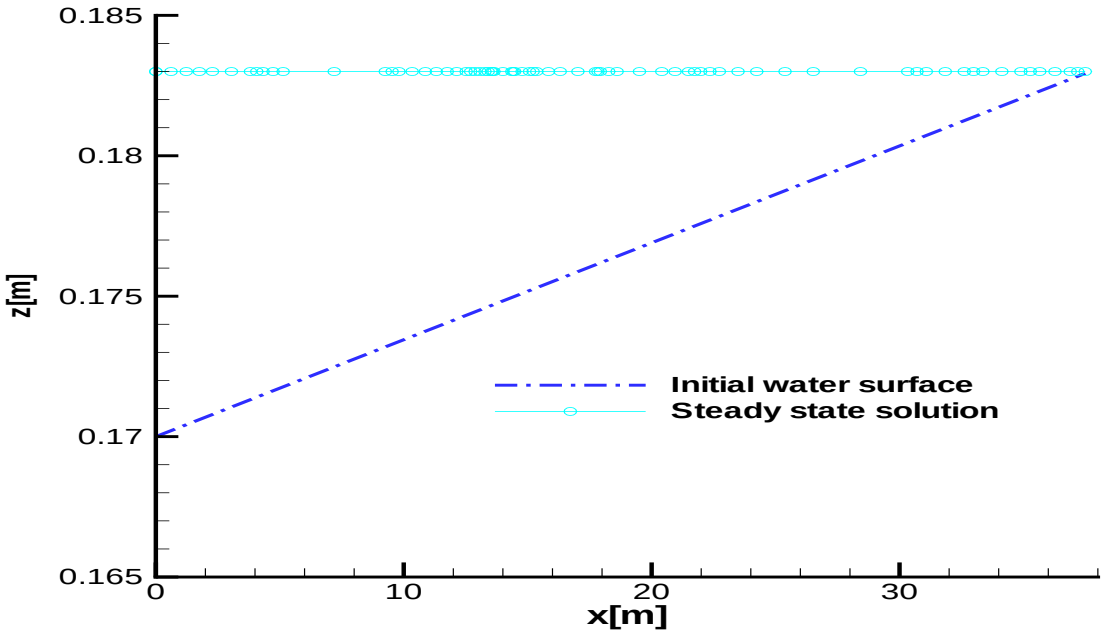

figure 8. Steady state solution and initial water surface along the channel

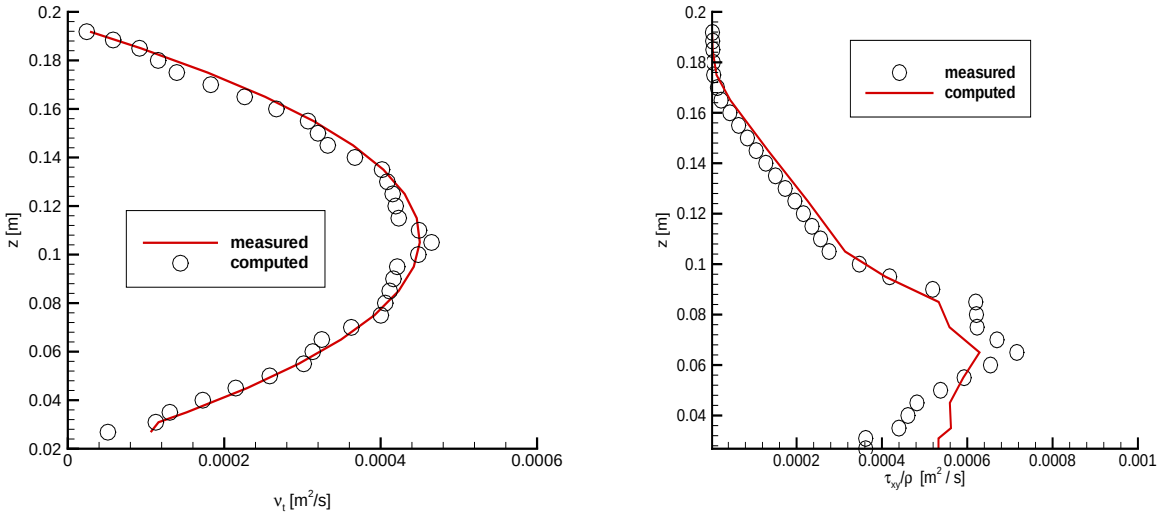

(a) (b)

figure 9. Comparison between computed and measured distributions at Inlet (x=0.01[m]) :

a) eddy viscosity

b) shear stress

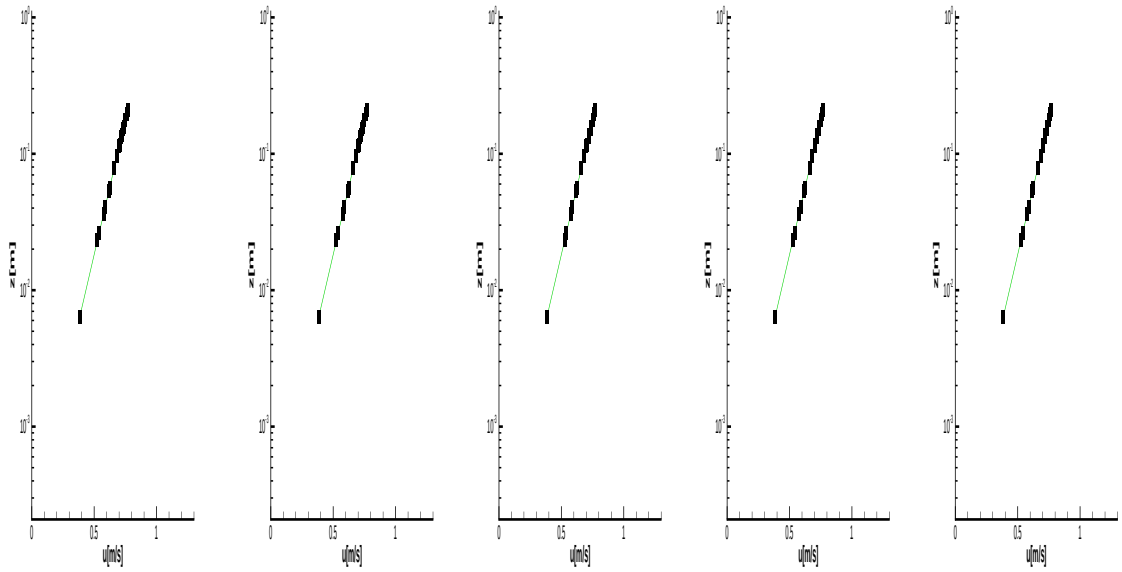

x=0.01[m] x=9.23[m] x=19.04[m] x=28[m] x=37.8[m]

figure 10. Steady state velocities distributions at selected sections

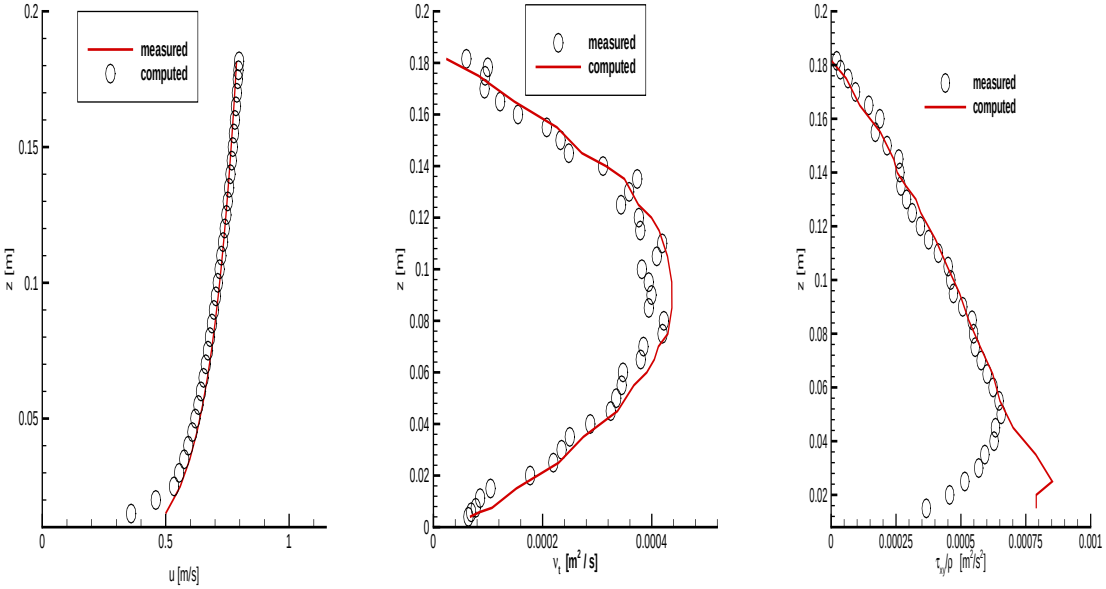

figure 11. Comparison betwween computed and measured distributions of velocity, eddy viscosity and shear stress

6.2 Unsteady open-channel flow

The channel layout and dimensions is shown in figure (12). The channel is 18[m] long, the width is $B = 0.60[m]$. The discharge is given by the hydrograph shown in figure (13).

The rough bed has an equivalent roughness height, $k_s = 0.0058[m]$. The flow depth at the outflow (donwstream end of the flume) is $0.13[m]$. The experimental data are available for the flow case (see [27]). The grid is composed of 3216 elements and 1802 nodes and the time step is $\Delta t = 0.1[s]$. The following pictures in figure (14) shows at two stations $x = 10.78[m]$ and $x = 14.08[m]$, the comparison between computed solution and measured time variation of flow depths. The model produces the surface ondulation as expected for the non-uniform flow.

Figure (15) shows the comparison between computed and measured distributions of the velocity, the eddy viscosity, and the shear stress at two stations $x = 10.78[m]$ and $x = 14.08[m]$ at time T=700[s]. The computed velocity distribution and eddy viscosity profile compares favorably with the experimental one. The eddy viscosity goes to zero near the free-surface, increases with the depth with a maximum around the mid-depth, and decreases towards zero near the bed. The shear stress profile is linearly distributed with the depth and from zero at the free surface goes to maximum near the bed. Figs. (16) and (17) shows good agreement between computed and measured kinetic energy and its rate of dissipation at the selected sections.

As shown in figures the computed solutions agree well with the experimental data.

7 Conclusion

In this work we proposed a semi-implicit 3D finite element scheme for $k - \epsilon$ turbulence models. The k and ϵ scalar fields are represented using a piecewise finite element based on flux conservation in the prism. This choice, combined with the Raviart-Thomas finite element for the velocity field, leads to a simple algebraic formulation. At each time step it is only required to solve a set of symmetric and tridiagonal matrices for the fluxes. Moreover the use of the upwind scheme (characteristics Galerkin method),the conservative form of the scalar equations, and fractional step method allows us to preserve the positivity of k, ϵ, the mass balance and the stability of the algorithm. The full scheme was used to test case approaching steady uniform flow measured by Istiarto [26] and the unsteady non-uniform flow measured by Qu [27]. The tests were performed in order to validate the model against well-known flow cases. A good agreement is found between the computed and measured flow fields.

Acknowledgment

One of us (C.Leupi) acknowledges the financial support of the Swiss National Science Foundation through grant number $21 - 65095 \cdot 01$.

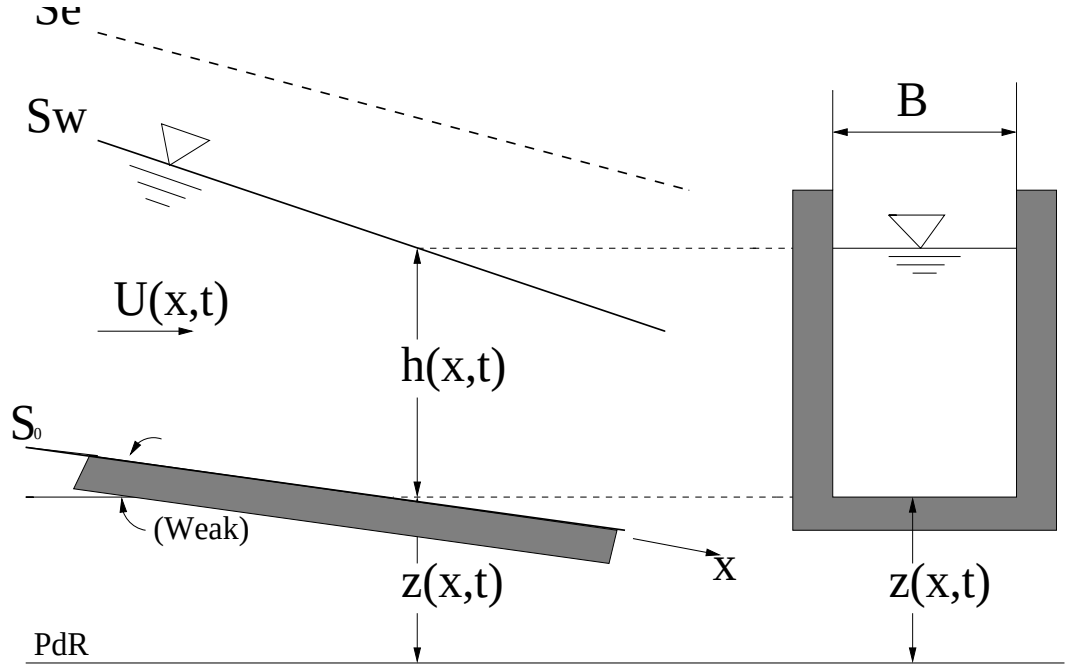

figure 12 Unsteady open−channel

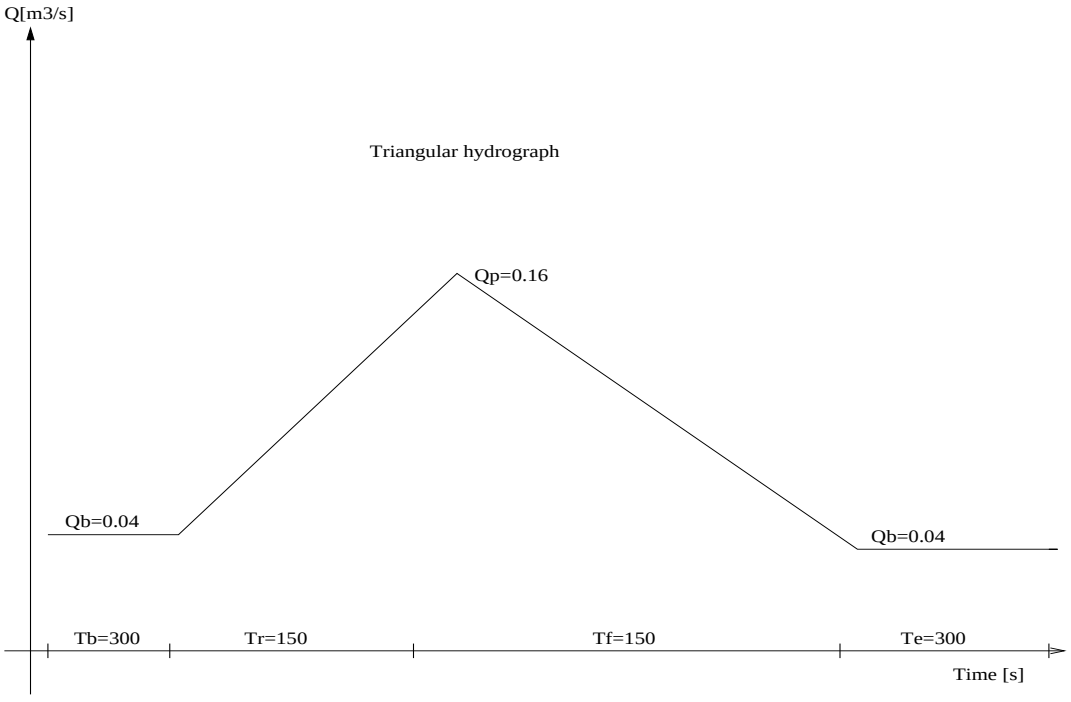

figure 13 Triangular hydrograph

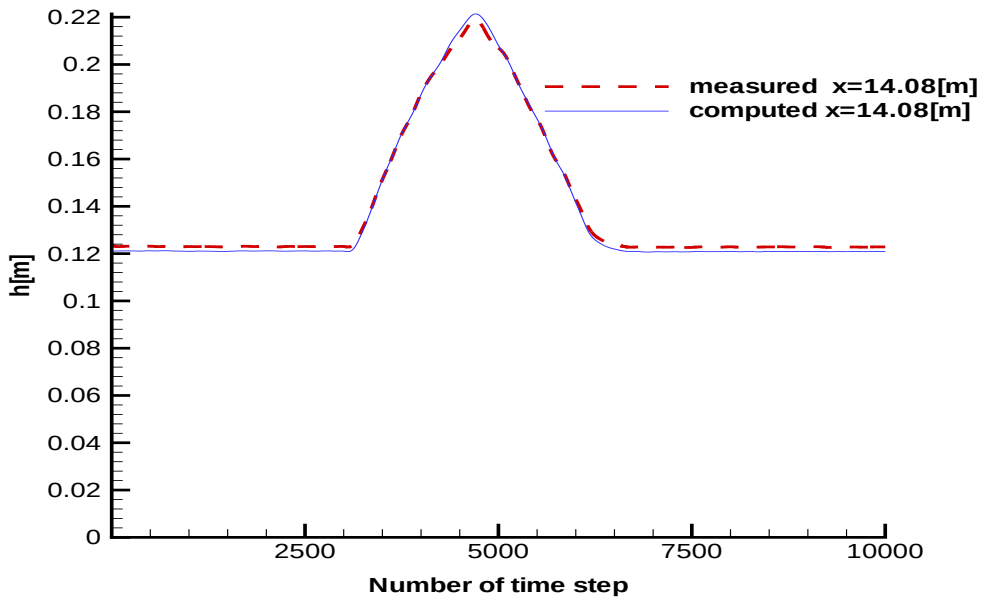

figure 14a.

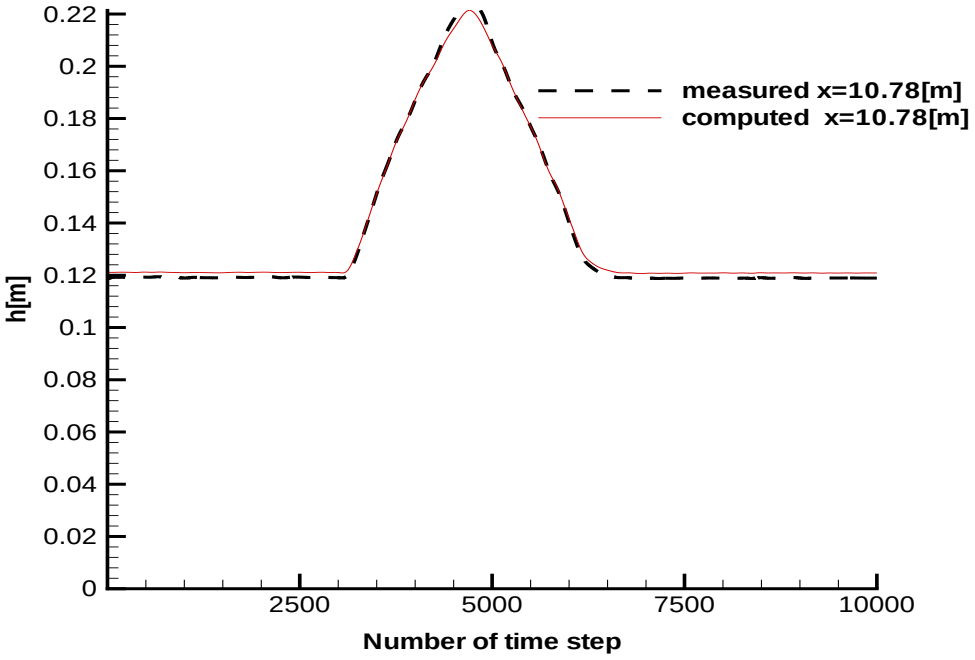

figure 14b.

Comparison between numerical and experimental time variation of depth of water :

a) x=10.78 [m]

b) x=14.08 [m]

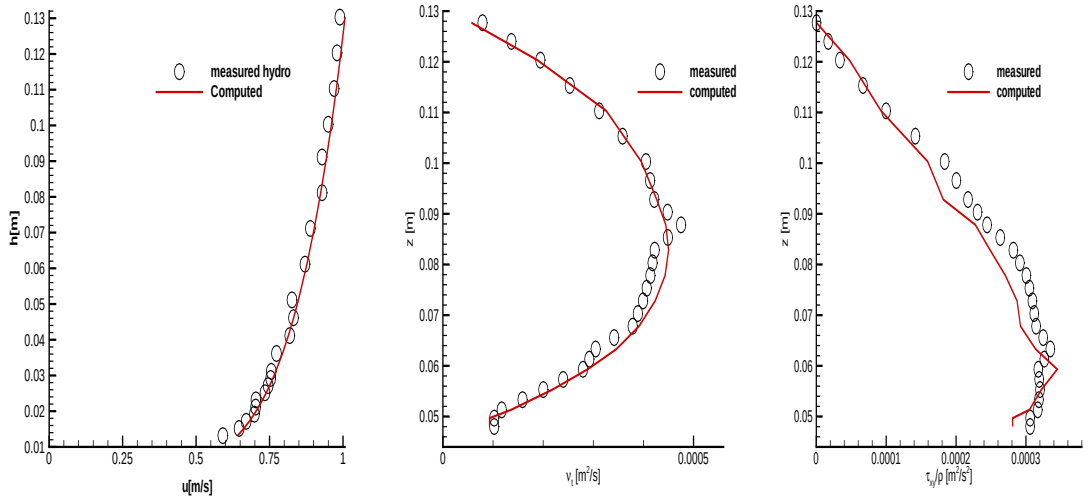

figure 15a

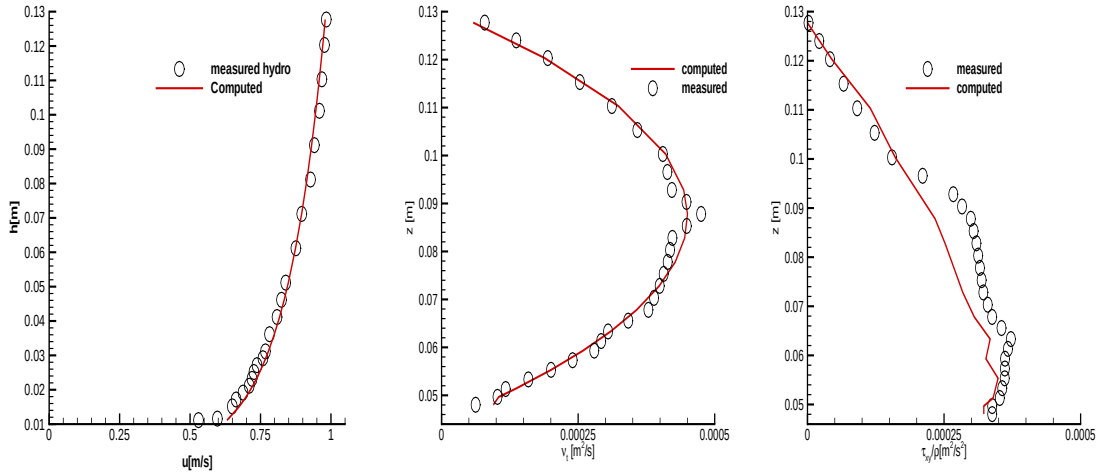

figure 15b.

Comparison of numerical (−) and experimental (o) results for velocity, eddy viscosity and shear stress:

a) x=10.78 [m]

b) x=14.08 [m]

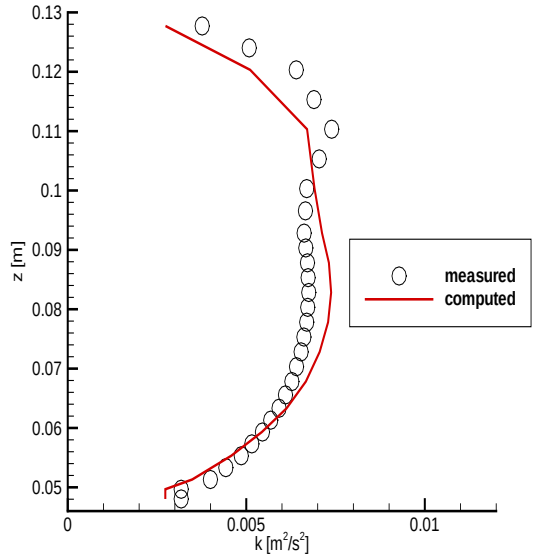

x=10.78[m]

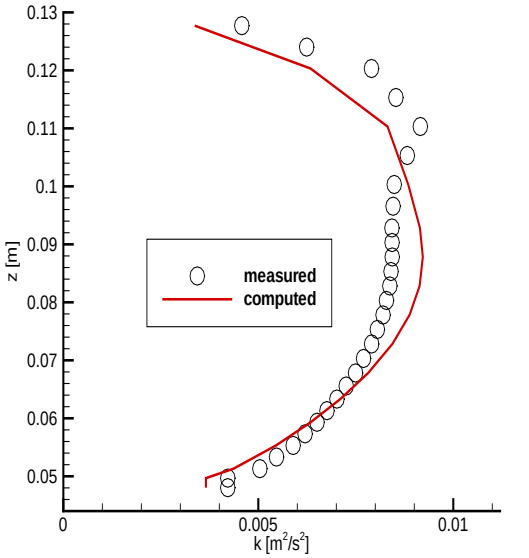

x=14.08[m]

figure 16 Computed and measured turburlent kinetic energy distributions at selected sections

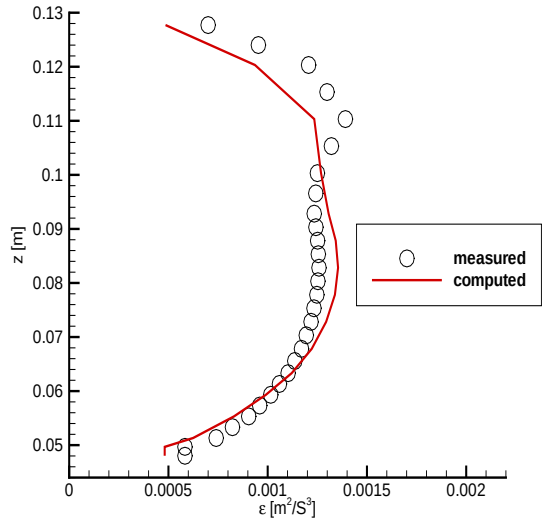

x=10.78[m]

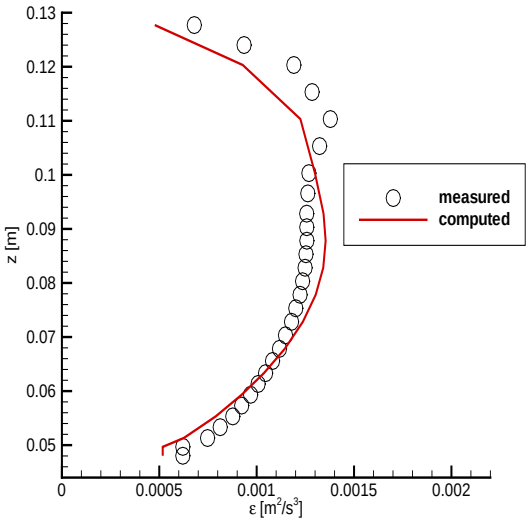

x=14.08[m]

figure 17 Computed and measured turburlent energy dissipation distributions at selected sections

References

[1] M. Kawahara, M. Kobayashi and K. Nakata (1983).*Multiple level finite element analysis and its implication to tidal current flow in Tokyo bay*,Appl. Math. Model.,7, 197-211.

[2] D. R. Lynch and F. E. Werner(1991). *Three-dimensional hydrodynamics on finite elements. PART II: Nonlinear time-stepping*, Int., J. Numer.Meth. Fluids,12,505-533.

[3] V. casulli and R., T., Cheng (1992). *Semi-implicit finite difference methods for three-dimensional shallow-water flow*, Int., J. Numer.Meth. Fluids, 15, 629-648.

[4] R. E. Uittenbogaard, J.A. Th. M. van Kester and G. S. Stelling. *Implementation of three turbulence models in 3D-TRIUSULA for rectangular grids*,Rep. Z81/Z162, Delft Hydraulics,1992

[5] P.K. Stansby and J.G. Zhou (1998)*Shallow-Water Flow Solver with Nom-hydrostatic Pressure: 2D vertical plane Problems* Int. J. Numer.Meth.Fluids 28: 541-563.

[6] Luyten P.J., Jones J.E., Proctor R., Tabor A.,Tett P. and Wild-Allen K.,(1999).COHERENS-*A Coupled Hydrodynamical-Ecological Model for Regional and Shelf Seas: User Documentation*. MUMM report,Management Unit of the Mathematical Models of North Sea, 914pp.

[7] C. G. Speziale (1987). *On non-linear $k-l$ and $k-\epsilon$ models of turbulence*, J. Fluid Mech., 178, 459-475.

[8] Sander, J. (1998). *Dynamical equations and turbulent closures in geophysics.* Continuum Mec. Thermodyn., 10:1-28.

[9] Canuto, V.M. (1994).*Large Eddy Simulation of turbulence : A subgrid scale model including shear, vorticity, rotation, and buoyancy*. Astrophys. J., 428:729.

[10] E. Miglio (2000). *Mathematical and Numerical Modelling for Environmental Applications* . Ph.D thesis, Department of Mathematics, University of Milano.

[11] Rodi W. (1987).*Examples of calculation methods for flow and mixing in stratified fluids*. J. Geophys. Res.,**92**, 5305-5328

[12] B. Mohammadi and O.Pironneau (1994) *Analysis of $k-$ epsilon Turbulence Model.* John Wiley & Sons, Chichester.

[13] E. Miglio , A. Quarteroni, and F. Saleri(1999) *Finite element approximation of Quasi-3D shallow water equations*, Comput. Methods Appl. Mech. Engrg., 174(34):355-369.

[14] Miglio,E. , A. Quarteroni, and F. Saleri(2003) *On the coupling of free-surface and groundwater flows*, Comput. Fluids, 32: 73-83.

[15] Roland, S.(1993) *Modélisation et simulation des Ecoulements turbulents.*, Hermes, Paris.

[16] Elder,J.W.(1959).*The dispersion of marked fluid in turbulent shear flow.* J. Fluid Mechanics, vol.5 ,544-560

[17] Shirou Aya(1991).*Longitudinal and Transverse Mixing in Open-Channel Flows* Report.

[18] Rodi W. (1980) *Turbulence models and their applications in hydraulics.* IAHR, Delft.

[19] Rodi W. (1984).*Turbulence models and their application in hydraulics. International Association for Hydraulic Research , 2nd, edition , Delft, Netherlands.*

[20] Launder, B.E., and Spalding, D.B.(1974).*The numerical computation of turbulent flows.* Comput. Meth. Appl. Mech. Engr.,3:269-289

[21] Peter K. Stansby (1996).*Semi-Implicit Finite Volume Shallow-water Flow and Solute Transport Solver With $k-\epsilon$ Turbulence.* Int. J. Num. Meth. Fluids,25:285-313.

[22] Wu, W., Rodi,W., and Wenka, T. (2000).*3D numerical modeling of flow and sediment transport in open channels.*ASCE, J. Hydr. Engrg., 126(1), 4-15.

[23] Cebeci,T. and Bradshaw,P. (1977)*Momentum Transfer in Boundary layers.* Hemisphere publi. Co., Washington, USA

[24] Versteeg, H.K. , and Malalasekera, W.(1995).*An introduction to Computational Fluid Dynamics: The Finite Volume Method.*, Longman Group, Essex, England

[25] P.A. Raviart and J.M. Thomas(1977) *A mixed finite element method for 2nd order elliptic problems*:I. Galligani and E. Magenes eds., Mathematical Aspects of Finite Element Methods, Lecture notes in Methematics(Springer-verlag), Berlin, 292-315.

[26] Istiarto, I. (2001). *Flow around a cylinder on a mobile channel bed.* PhD. thesis no. 2368, EPFL, Lausanne, Switzerland.

[27] Zhaosong Qu (2002). *Unsteady open-channel flow over a mobile bed.* PhD. thesis no. 2688, EPFL, Lausanne, Switzerland.